Revista Ciência Agronômica, v. 56, e202391928, 2025
Centro de Ciências Agrárias - Universidade Federal do Ceará, Fortaleza, CE
www.ccarevista.ufc.br

Scientific Article
ISSN 1806-6690

Modeling corn evapotranspiration using the SEBAL algorithm in the Peruvian highlands[1]

Yénica Cirila Pachac Huerta[2]*, Eduardo Chávarri-Velarde[3], Melania Mabel Zapana Quispe[4], Robinson Fabricio Peña Murillo[5]

ABSTRACT - The estimation of evapotranspiration (ET) and crop water requirements are crucial for the proper management and allocation of water resources in terms of quantity, quality, and timeliness. Therefore, remote sensing estimation of ET using the SEBAL algorithm (Surface Energy Balance Algorithm for Land) can provide spatio-temporal, non-punctual data, unlike traditional calculations relying on the nearest meteorological station. This research analyzed ET using SEBAL, based on ten Landsat 8 satellite images processed with a program developed in the Model Builder of ArcGis® version 10.2. The analysis was conducted during the vegetative period of starchy corn from May to October 2016. Validation of the results happened with a drainage lysimeter installed in a monitoring plot. Additionally, the statistical indices – such as percentage relative error (PRE) (0,09), root mean square error (RMSE) (0,30), R^2 (0,92), and Nash-Sutcliffe efficiency (NASH) (0,91) – indicated a good correlation of ET for starchy corn in the central highlands of Peru. The ET identified at ten monitoring points ranged from 1,05 to 7,79 mm d^{-1}.

Key words: Landsat. Lysimeter. Corn. Model Builder. Remote Sensing.

DOI: 10.5935/1806-6690.20250018
Editor-in-Chief: Prof. Salvador Barros Torres - sbtorres@ufersa.edu.br
*Author for correspondence
Received for publication 04/06/2023; approved on 21/11/2023
[1]Part of the first author's master's thesis. The work was supported by the Research Center for Development of the Santiago Antúnez de Mayo National University-Peru (UNASAM) and the Master's program in Water Resources of the La Molina National Agrarian University-Peru (UNALM)
[2]Faculty of Agricultural Sciences, Santiago Antúnez de Mayolo University (UNASAM), Huaraz, Peru, ypachach@unasam.edu.pe (ORCID ID 0000-0002-1577-0548)
[3]PhD and Master's Programs in Water Resources, Graduate School, National Agrarian University La Molina, Lima, Peru, echavarri@lamolina.edu.pe (ORCID ID 0000-0002-8445-8996)
[4]Faculty of Agricultural Engineering, National University of Altiplano, Puno, Peru, mzapana@unap.edu.pe, (ORCID ID 0000-0002-3412-4285)
[5]Faculty of Agricultural Sciences, Technical University of Ambato, Tungurahua, Ecuador, rf.pena@uta.edu.ec, (ORCID ID 0000-0001-6196-4039)

INTRODUCTION

Studies have shown that over 60% of the precipitation reaching the surface through condensation returns to the atmosphere via the processes of evaporation (E) and evapotranspiration (ET). This proportion can rise to as much as 90% due to decreased precipitation and increased ET in arid areas (Yang *et al.*, 2022). This loss of water from the Earth's surface to the atmosphere serves as a connection between the cycles of water, energy, and carbon, as well as ecological and hydrological processes (Aryalekshmi *et al*., 2021; Guo *et al*., 2022; Hu *et al.*, 2021; Yang *et al.*, 2022).

In agriculture, water is mainly consumed as ET (Paredes *et al*., 2017) , which is a crucial part of energy transfer, and has an impact on the growth and development of plant roots (Tan *et al.* , 2021).

Remote sensing (RS) is valuable for mapping both small and large areas (Ali *et al.*, 2021). In comparison to in situ observations, RS measurements augment regional-scale data, especially in locales with scarce meteorological data, such as ET and surface soil moisture (Guo *et al.*, 2022). Moreover, RS is also beneficial in estimating parameters like albedo, Normalized Difference Vegetation Index (NDVI), and Leaf Area Index (LAI) (Aryalekshmi *et al*., 2021).

The Surface Energy Balance for Earth (SEBAL) algorithm is a widely applied model for estimating ET using RS data and exhibits relatively high simulation accuracy. This model utilizes a hybrid approach that blends empirical and physical parameterization schemes (Prakash; Rajitha; Varma, 2020; Wei *et al*., 2022). The estimation of crop ET is carried out without the use of potential evapotranspiration (PET) or a tabulated crop coefficient (Kc) (Aryalekshmi *et al.*, 2021). It is an algorithm developed by Bastiaanssen *et al.* (1998) and later enhanced by Allen *et al.* (2005) to estimate ET in terms of the instantaneous surface energy balance (Tan *et al.*, 2021). Due to its versatility, it has been used to estimate the ET of various crops around the world such as sugarcane (Goshehgir; Golabi; Naseri, 2021; Kiptala *et al.*, 2018) and maize in Iran (Kamyab; Mokhtari; Jafarinia, 2022) and Turkey (Shamloo *et al*., 2021).

The accuracy of the ET estimated by SEBAL has been investigated and can reach 85% for daily ET (Laipelt *et al.*, 2021), 95% for field-scale station-wide ET, and 96% for annual ET in large catchments (Shamloo *et al*., 2021; Wei *et al.*, 2022). Also, it has been developed in over 30 countries, such as Saudi Arabia, Brazil, China, the United States, Egypt, Ghana, India, Iran, and Italy, due to its low dependency on soil data. According to Cha, Li y Wang (2020), in countries like China, India, Spain, and Pakistan, results have shown that the accuracy of the estimated ET is consistently 85%, even when compared with uncalibrated field measurements, thereby yielding consistent and accurate results.

Here we aimed to estimate the ET of the starchy corn (*Zea mays* L.) crop using RS techniques and the SEBAL algorithm under the conditions of the Peruvian mountains (Huaylas Valley) during the year 2016.

MATERIAL AND METHODS

Figure 1 illustrates the methodological progression of the research, beginning with the collection of field data and acquisition of Landsat 8 Operational Land Imager (OLI) satellite images. Both were biweekly monitored during the crop's vegetative period. Subsequently, the SEBAL algorithm was employed to estimate crop ET.

The study area is located in Peru, Ancash department, in the Santa River basin, in the open Andean valley of Huaylas north of Lima, between the Pacific Ocean and the Marañón River, between important mountain ranges, the Cordillera Blanca and the Negra, between the provinces of Carhuaz and Yungay (Figure 2a-b). Between the latitudes and longitudes of 9º20'00''-9º40'00''S and 77º33'00''-77º48'00''W, respectively. It has an average elevation of 2600 m, slopes less than 20º, semi-dry and temperate climate, with summer rainfall (October to March) ranging from 300 to 700 mm annually, with maximum temperatures between 21 to 28 °C and minimum temperatures of 2 to 9 °C, temperatures decrease with height at a rate of 0,5 ºC for every 100 meters (Cubas *et al*., 2013). The main tributary is the Santa River, which flows from south to north. Its lands are very rich for agriculture and there are currently large fields of corn, potatoes, flowers, and fruit trees; in the area under study, 85% of starchy corn with dry and green grains predominates. Corn, along with rice and wheat, is considered the most cultivated cereals in the world and is one of the foods that guarantee food security for the population (Garcia *et al.*, 2007). In turn, in Peru alone, a production of 818 983.91 t of corn was obtained in 2022, representing the fourth product with the highest production in the country (Peru, 2022).

Satellite images and Digital Elevation Model

Ten Landsat 8 OLI images were used, which were downloaded biweekly throughout the vegetative period of starchy corn, a crop planted in the experimental plot from May 14 to October 5, 2016, with cloudiness less than 50%. The images were obtained from the United States Geological Survey (USGS), Global Visualization Viewer (GloVis) server, available at https://glovis.usgs.gov/app?fullscreen=1.In all images, the approximate capture time was 15:16 UTC (Coordinated Universal Time), and the column and row were 8 and 66, respectively (Table 1),

and the characteristics of the bands are presented in Table 2. The Digital Elevation Model (DEM) was generated based on the national chart scale of 1:100000 available at http://sigmed.minedu.gob.pe/descargas/.

The two meteorological stations utilized, Tingua and Cañasbamba (Figure 2-c), as well as the radiometer (Figure 2-d), are part of the Environmental Research Center for Development at Santiago Antúnez de Mayolo National University (CIAD-UNASAM). Data on precipitation, temperature, radiation, and evaporation were collected daily and evaluated biweekly, enabling the estimation of PET using the ETR.REF software that employs the standardized Penman-Monteith method.

Figure 1 - Methodological outline of the research

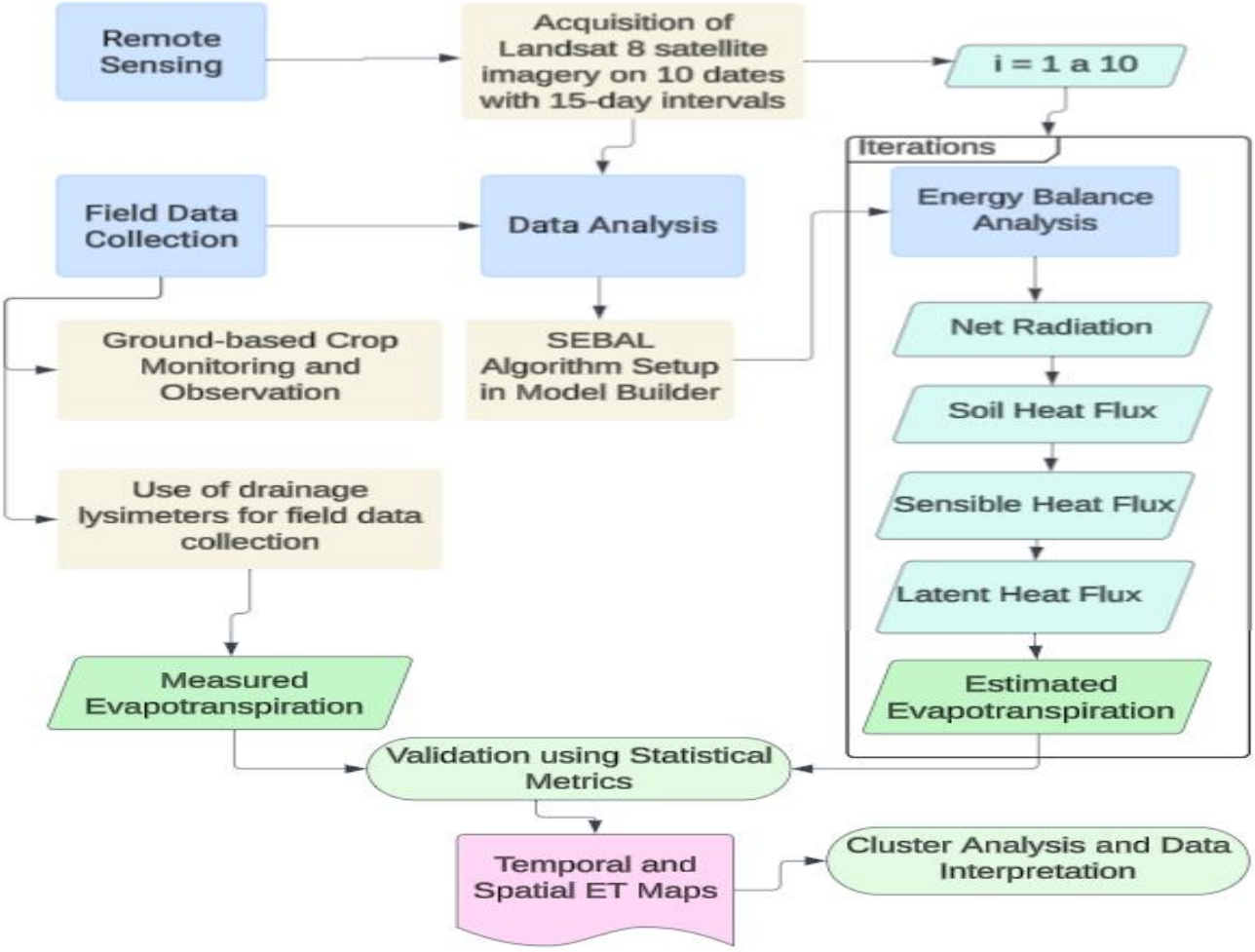

Table 1 - Data from the 10 Landsat 8 OLI satellite images

Image No.	Date	Time (UTC)	Image No.	Date	Time (UTC)
1	14-May-2016	15:15:52.85	6	2-Aug-2016	15:16:21.44
2	30-May-2016	15:15:59.49	7	18-Aug-2016	15:16:25.75
3	15-Jun-2016	15:16:01.93	8	Sep 3, 2016	15:16:32.02
4	1-Jul-2016	15:16:11.20	9	Sep 19, 2016	15:16:34.32
5	17-Jul-2016	15:16:18.09	10	5-Oct-2016	15:16:36.61

Table 2 - Characteristics of the Landsat 8 OLI sensor bands

Band	Sensor	Wavelength Spectral resolution (µm)	Radiometric resolution (bits)	Spatial resolution (m)	Temporary resolution (days)
Band 1 - coastal aerosol	OLI	0.43 – 0.45	16	30	16
Band 2 - blue	OLI	0.45 – 0.51	16	30	16
Band 3 - green	OLI	0.53-0.59	16	30	16
Band 4 - red	OLI	0.64 – 0.67	16	30	16
Band 5 - Near Infrared (NIR)	OLI	0.85-0.88	16	30	16
Band 6 - Shortwave Infrared (SWIR) 1	OLI	1.57-1.65	16	30	16
Band 7 - Shortwave Infrared (SWIR) 2	OLI	2.11 to 2.29	16	30	16
Band 8 - Panchromatic	OLI	0.50-0.68	16	15	16
Band 9 - Cirrus	OLI	136 – 1.38	16	30	16
Band 10 - Thermal Infrared (TIRS) 1	TIRS	10.60 – 11.19	16	100	16
Band 11 - Thermal Infrared (TIRS) 2	TIRS	11.5 – 12.51	16	100	16

Note: OLI = Operational Land Imager, TIRS = Thermal Infrared Sensor, band 11 was resampled to 30 m

Concurrent with the data collection in the experimental plot, 11 points (PM) distributed across the analysis area were monitored. These points featured both dry and green starchy corn crops in various phenological stages (initial, medium, and maturation), reflecting the farmer's initial decision when planting the crop (Figure 2-c). Points 10 and 11 were located within the experimental plot (Figure 2-d).

The calibration of the SEBAL model was carried out by monitoring the vegetative period of starchy corn in a 2 ha experimental plot at the Cañasbamba Research Center. A radiometer and drainage lysimeter were installed in the plot to measure radiation and ET respectively (Figure 2-d). The starchy corn variety was chosen due to its lengthy vegetative period of 5 to 6 months and its higher resistance to pests and diseases.

SEBAL methodology

The SEBAL methodology, proposed by Bastiaanssen *et al.* (1998), is a robust tool for estimating ET based on RS data. SEBAL calculates the ET in terms of latent heat flux (λET), using a surface energy balance, integrating net radiation (R_η), soil heat flux (G) and sensible air heat flux (H). The energy balance is expressed by equation 1.

$$\lambda ET = R_\eta - G - H \quad (1)$$

SEBAL has been studied and explained in detail, from input data such as elevation, satellite imagery, and meteorological data to the final derivation of ET to Bastiaanssen *et al.* (1998), Ghaderi *et al.* (2020), Rahimzadegan y Janani (2019) y Waters *et al.* (2002). The calculation performed to obtain λET was for each pixel included in the study area and the ten images analyzed, so automated programming was performed in Model Builder of ArcGis® ESRI version 10.2, to streamline geospatial workflows for repetitive and iterative calculations required in the analysis. Figure 3 shows the toolbox with the model elements (tools, variables, connectors), which contains 18 models representing the steps required for estimating the ET of the analyzed satellite images.

Validation of evapotranspiration results

To validate the ET estimated using the SEBAL algorithm, we compared it with measurements taken from a drainage lysimeter with dimensions of 1.20 m in length, 0.80 m in width, and 1 m in height. We installed this lysimeter in an experimental plot where starchy corn was being grown under similar field conditions. A container was positioned under the lysimeter to collect the drained water. We recorded both the inflow and outflow from the lysimeter to determine the ET in the field, taking into account factors like irrigation, humidity, and drainage. We derived the daily value, which is expressed in millimeters per day, by subtracting the stored irrigation depth and the drained depth from the applied irrigation depth, as narrated in the article by Lyles *et al.* (2024).

To validate the congruence between the measured and estimated values employing the SEBAL algorithm, statistical metrics like Pearson Correlation (PRE), Root Mean Square Error (RMSE), Coefficient of Determination (R^2), and Nash-Sutcliffe Efficiency (NASH) were utilized. The specific equations for these statistics are detailed meticulously in Ferreira, Paz, and Bravo (2020).

Fundamental approaches to data clustering in statistical and machine learning analysis

Figure 2 - Location of (a) Ancash Department in Peru, (b) location of the study area in the provinces of the Huaylas alley, (c) study area in yellow line, Tingua and Cañasbamba meteorological stations in green triangles and the 11 monitoring points (MP) in red dots and (d) limit of the Cañasbamba Experimental Center (red line), experimental plot (green fill) in which the drainage lysimeter and radiometer were located

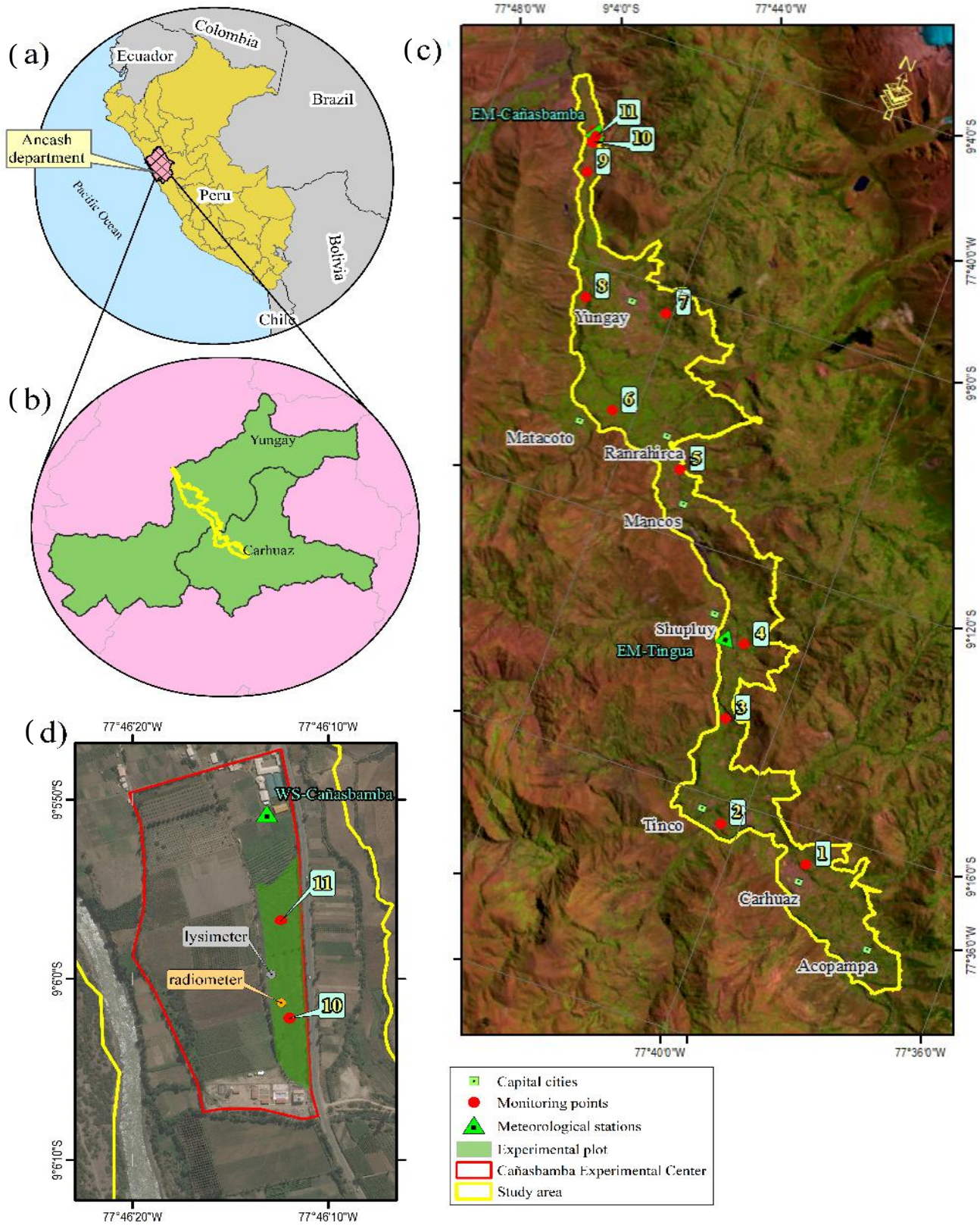

Figure 3 - Model Builder design prepared for SEBAL processing

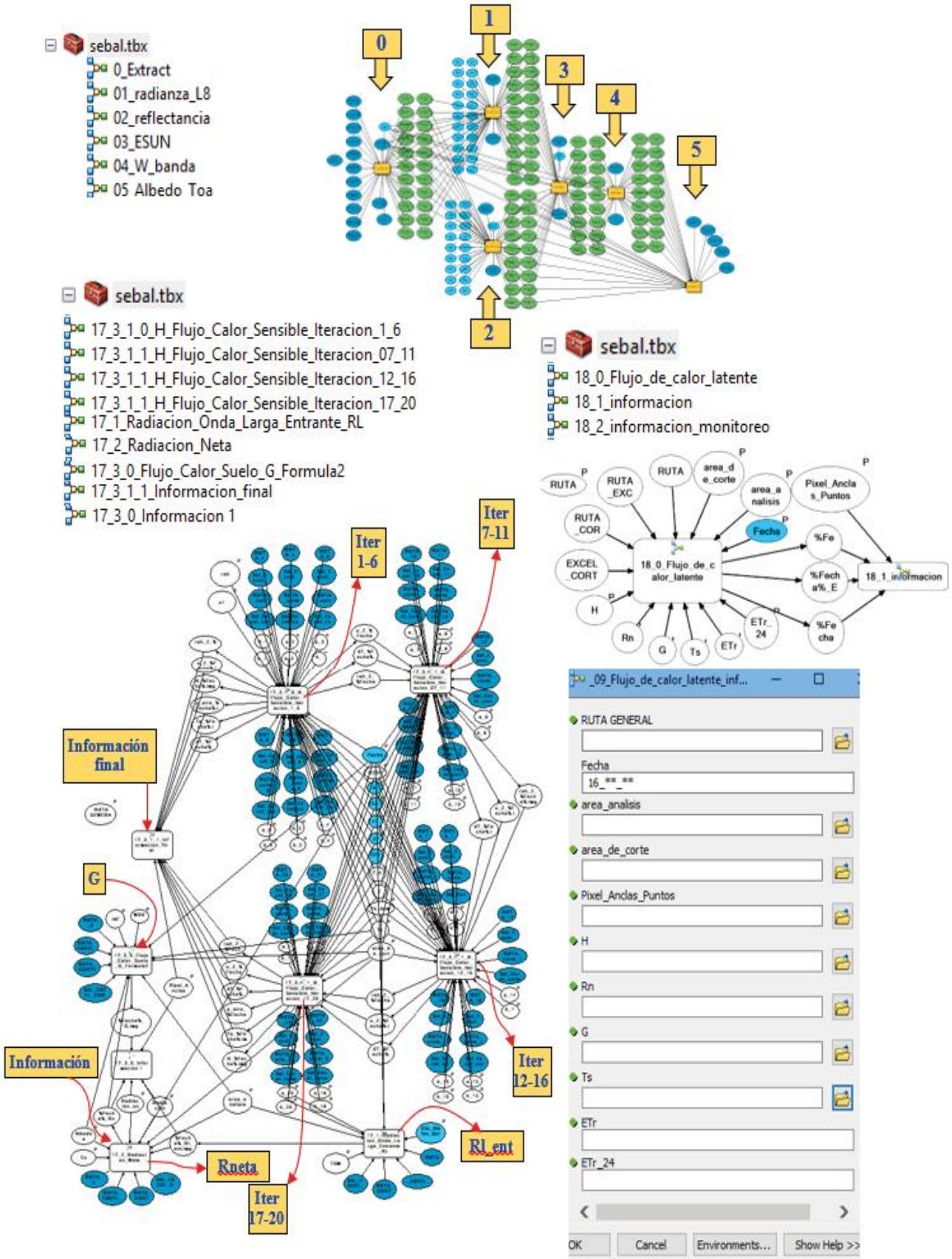

K-means cluster analysis is a widely-used technique to partition a dataset into k clusters, where each observation belongs to the cluster with the nearest centroid. This technique is efficient and easy to implement, but it requires pre-specification of the number of clusters (k). The algorithm iteratively assigns points to the nearest centroids and recalculates the centroids until the assignments no longer change. It is also worth mentioning that hierarchical cluster analysis is another popular technique that does not require pre-specification of the number of clusters. Specifically, the Ward.D2 method stands out for its ability to minimize the total variance within clusters. It begins with each observation in its cluster and merges the two clusters resulting in the smallest increase in the sum of squared errors at each step. This process produces a dendrogram, which is a tree-like visual representation of the hierarchical relationships between observations. It enables the identification of cluster structures at different levels of aggregation (Soetewey, 2024).

RESULTS AND DISCUSSION

Selecting the representative pixel for product evaluation:

This study analyzed ten Landsat 8 satellite images, each with a spatial resolution of 30 meters, captured between May 14 and October 5, 2016. The aim was to evaluate the behavior of ET during the phenological period of the starchy corn crop in Callejón de Huaylas, located in the Peruvian highlands. The choice of starchy corn as a subject of this study was dictated by its profitability, low requirements for manual labor, and easily accessible location. As depicted in Figure 2c, the study area is conveniently positioned near the main interprovincial transport route and is sown with both dry and green starchy corn throughout the year. The analysis revealed variations in ET during the maize growth cycle. This essential data can potentially improve irrigation practices and overall water management in regional agriculture. The results affirm that satellite imagery is an effective tool for monitoring ET, significantly contributing to water resource sustainability and agricultural planning in the Callejón de Huaylas.

The results were validated using the drainage lysimeter situated in the experimental plot of the Cañasbamba Research Center (see Figure 2d). It was determined that the ET estimated with SEBAL corresponds to PM 10 (as shown in Table 3), given that it is the crop closest to the lysimeter. Figure 4 presents the temporal variation of the experimental plot from the initial to the development, middle, and final stages.

Figure 4 - Temporal variation of starchy corn phenology in the experimental plot (Parc) and drainage lysimeter (Lis) at the stages of (a) beginning, (b) development, (c) middle, and (d) end

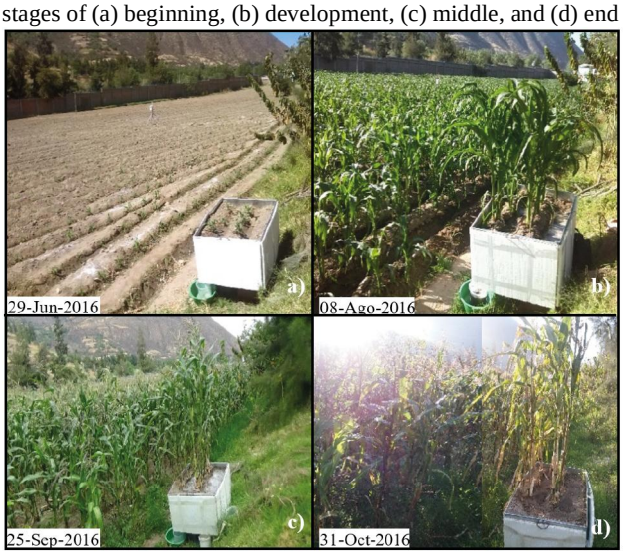

Table 3 - Time values of the variation of the components of the SEBAL algorithm

Date	α	Rn (W m^{-2})	G (W m^{-2})	H(W m^{-2})	LE (W m^{-2})	PET Cañ (mm d^{-1})	PET Tin (mm d^{-1})	ET PM10 (mm d^{-1})	ET Lis (mm d^{-1})
14 -May-2016	0.20	523	93	312	118	6.7	6.8	1.4	NA
30-May-2016	0.20	497	94	262	141	6.6	6.9	1.9	NA
15-Jun-2016	0.19	496	90	196	210	6.4	6.7	3.1	2.7
01-Jul-2016	0.20	486	84	189	213	6.2	6.4	3.1	2.8
16-Jul-2016	0.17	518	87	198	233	6.2	6.4	3.2	2.9
02-Aug-2016	0.15	563	91	188	284	5.7	6.2	3.5	3.2
18-Aug-2016	0.13	608	102	191	315	7.2	7.3	4.8	4.4
03-Sep-2016	0.12	662	108	160	394	7.4	7.8	6.0	5.9
19-Sep, 2016	0.13	680	101	247	332	7.6	7.0	4.1	4.4
05-Oct-2016	0.14	702	104	270	328	5.5	5.5	2.8	3.1

Note: α is the dimensionless albedo, Rn is the net radiation, G is the ground heat flux, H is the air heat flux, and LE is the Latent Heat Flux, all expressed in W m $^{-2}$ all calculated in PM10. PET indicates the Potential Evapotranspiration of the Cañasbamba (Cañ) and Tingua (Tin) Meteorological Station, expressed in units of mm d $^{-1.}$ Evapotranspiration (ET) values are represented for the SEBAL algorithm in the experimental plot (Parc) and Drainage Lysimeter (Lis) expressed in mm d $^{-1.}$ NA indicates an undetermined value

The PET obtained for the meteorological stations indicates similar behavior, although it is slightly higher in Tingua (EM Tin) compared to Cañasbamba (EM Cañ). Given that EM Tin is situated at a higher elevation than EM Cañ, this can be explained in line with Bennie *et al.* (2008), who postulate that PET tends to decrease with elevation because of a decrease in air temperature. Nevertheless, they also acknowledge that other factors, such as incident solar radiation and wind speed, can influence this relationship due to local conditions (Figure 5).

Figure 5 - Spatio-temporal variation of evapotranspiration (ET) in mmd $^{-1}$ in the study area (Figure 2c) during the analysis period, (a) 14-May-2016, (b) 30-May-2016, (c) 15-Jun-2016, (d) 01-Jul-2016, (e) 17 Jul-2016, (f) 02-Aug-2016, (g) 18-Aug-2016, (h) 03-Sep-2016, (i) 19-Sep-2016, (j) 05-Oct-2016. The variation of the ET ranges from 0 mm d $^{-1}$ to 10 mm d $^{-1}$

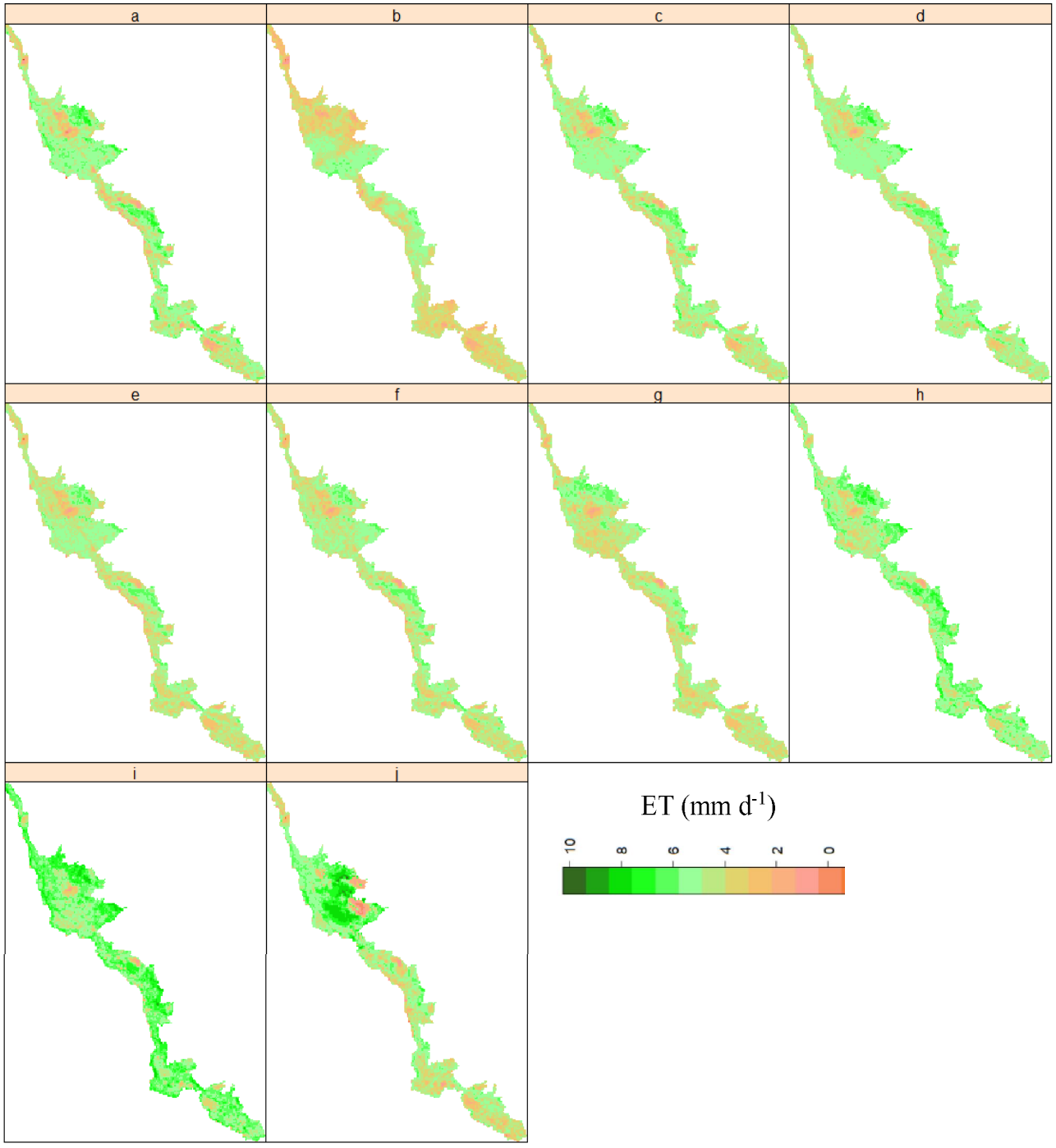

Analysis of Rn, G, H

In the experimental plot (PM10 located 25 m from the radiometer), Rn values were found to range from 486 to 710 W m -2. This is consistent with those suggested by Waters *et al*. (2002), who indicated that the Rn range is between 100–700 W m^{-2}, depending upon the spatial and temporal location of each cell in the raster. However, on 05/10/2016, results exceeded this range (Table 3). Rn is related to both short and long-wave radiation, which are in turn directly related to surface temperature. In areas where the surface temperature is high, the radiation is also high. Conversely, radiation has an inverse relationship with albedo (Rahimzadegan; Janani, 2019).

The heat flux (H) is lower during the longest vegetative period due to the excessive absorption of radiation by the large leaf area. It tends to reach its peak during the day and decrease in the afternoon. These results are consistent with the research conducted by Zhang *et al.*, 2010, who recorded maximum values of up to 300 W m^{-2} in a corn crop field. Meanwhile, the ground heat flux (G) varies from 66 to 108 W m^{-2}, demonstrating little variability on the reference scale of net radiation (Rn) and H.

The ET estimate, obtained through SEBAL from the pixel nearest to the drainage lysimeter (PM10), demonstrates that the net radiation (Rn) peaked from September to October. The soil heat flux (G) remains consistent throughout the temporal analysis, while the sensible heat flux (H) recorded its lowest levels in September. Consequently, as a result of the energy balance, the latent heat flux (LE) reached its peak during the maximum vegetative period of the monitored crop on September 3, 2016 (Figure 6a and Table 3).

These results are consistent with those indicated by, those who investigated that the increase in ET in some areas was mainly related to the increase in wind speed, which is also related to greater net solar radiation and air surface temperature. Ruiz *et al.* (2011) indicate that the increase in temperature also modifies the ET rates, which generates an increase of 3.4% for each degree Celsius of increase; consequently, it influences the decrease in precipitation and the reduction of land suitability and economic performance (Kimball, 2015).

Importance of monitoring points

The spatio-temporal variation of ET in the study area, analyzed at 11 PM over 10 dates, ranged from a minimum of 1.05 to a maximum of 7.79 mm d^{-1} The spatiotemporal variability indicates a clear representation of different sowing dates in the study region. Given that the land is owned by various farmers, even those with minimum areas of 120 m^2, market demand can influence the start of sowing intentions on different dates. Cluster analysis revealed that the ET varies due to the sowing date, latitude, and elevation. This analysis determined that the 11 PM are distributed into four groups with different characteristics (Figure 7). As evident in Table 4, groups 1, 2, 3, and 4 reached their maximum values during the middle phase in September, with ET values of 6.00 mm d^{-1}; 7.79 mm d^{-1}; 5.45 mm d^{-1}; 5.23 mm d^{-1} respectively. Additionally, groups 2, 3, and 4 presented an additional middle phase in May, with maximum ET values of 6.00 mm d^{-1}; 5.49 mm d^{-1} and 5.88 mm d^{-1} respectively (Figure 8).

Table 4 presents the ET results for various experimental groups dealing with starchy corn. Group 1, composed of measurement points PM10 and PM11, is situated at latitudes 9°6’01’’ and 9°5’56” respectively and shows an average ET of 3.47 mm d^{-1} and 3.29 mm d^{-1}. These findings aptly demonstrate that ET can vary spatiotemporally in adjacent plots, as these plots exhibited distinct growth patterns due to differing soil types.

Group 2, which comprises measurement points PM1, PM4, and PM7, is installed with green-grain starchy corn at elevations higher than 2550 m. The

Figure 6 - Temporal variation of (a) potential evapotranspiration from the Tingua (EM Tin) and Cañasbamba (EM Cañ) meteorological stations, represented by filled and unfilled circles respectively; (b) Components of the SEBAL algorithm (Surface Energy Balance Algorithm for Land) such as net radiation (Rn), soil heat flux (G), sensible air heat flux and latent heat flux (LE), are represented by filled rhombus, unfilled square, unfilled rhombus and filled square respectively, all calculated in PM10

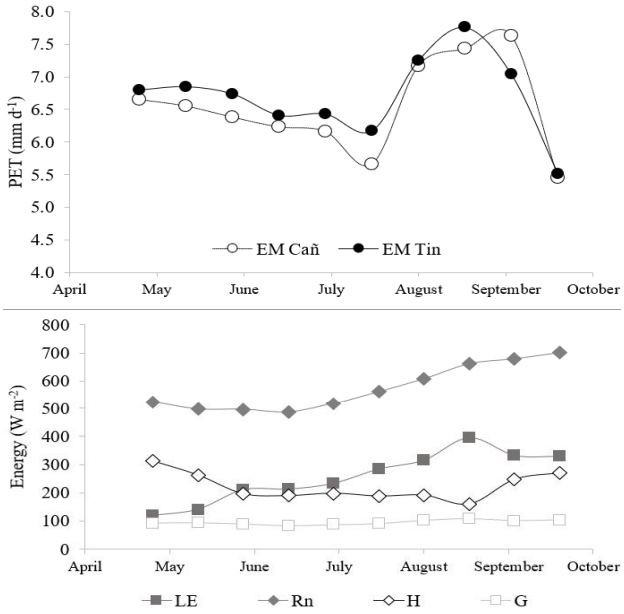

latitudes range between 9°8'23'' and 9°16'37''. This group shows the highest average ET values across the analysis area, with 4.53 mm d^{-1}, 5.39 mm d^{-1} and 5.57 mm d^{-1} respectively.

Group 3, which also has green starchy corn, includes the PM2, PM3, and PM5 measurement points. These points are situated at elevations between 2450 and 2600 m, and latitudes greater than 9°10' S. They exhibit average ETs of 4.19 mm d^{-1}, 4.05 mm d^{-1} and 4.52 mm d^{-1} respectively.

Finally, Group 4 – which includes measurement points PM6, PM8, and PM9, located at latitudes lower than 9°10' S – represents the second group with the highest average ET. The respective values for these points are 4.82 mm d^{-1}, 4.58 mm d^{-1} and 4.11 mm d^{-1} respectively.

The current study bolsters Bennie *et al*. (2008)'s findings, asserting that ET at higher elevations can be augmented by specific local conditions such as solar radiation and wind speed. These factors may counterbalance the general trend of ET diminishing at greater altitudes.

The four groups display distinct phenological behaviors. Groups 1 and 2 showcase similarity in their sowing dates, such that both groups reach a maximum ET in September (middle phase). Group 2 exhibits the highest values, primarily due to the crops being planted at high elevations. In contrast, groups 3 and 4 consist of crops with two phenological periods identified within the same crop type (green-grain starchy corn). The initial monitoring phase in Group 1 aligns with the middle phase of groups 3 and 4, suggesting that at lower latitudes, the ET is higher (Figure 8).

From the analysis of the phenological phases of the four groups, we found that the developmental phase had an average ET of 3.27 mmd^{-1}; 5.35 mm d^{-1}; 4.02 mm d^{-1} and 4.44 mm d^{-1} respectively. Meanwhile, the middle phase had an average ET of 5.95 mm d^{-1}; 5.79 mm d^{-1} ; 4.69 mm d^{-1} and 5.26 mm d^{-1} respectively (Figure 9).

The results show that ET exhibits spatial and temporal variability due to a range of factors, including precipitation, solar radiation, air and surface temperature, wind speed, soil hydraulic characteristics, elevation, land use, and vegetation types among others (Aryalekshmi *et al.*, 2021; Tan *et al.*, 2021). Consequently, accurate and swift estimation of ET is vital for assessing, planning, optimizing, monitoring, and managing water resources consumption (Ali *et al.*, 2021; Asadi; Kamran, 2022; Kamyab; Mokhtari; Jafarinia, 2022), as well as for hydrology, climatology (Aryalekshmi *et al.*, 2021), meteorology, and geography (Yang *et al.*, 2022).

Table 4 - Maximum daily evapotranspiration (grey fill) and average (green fill) estimated with the SEBAL algorithm in the four identified groups; Group 1 (PM 10 and 11), Group 2 (PM 1, 4 and 7), Group 3 (PM 2, 3 and 5) and Group 4 (PM 6, 8 and 9)

Cluster	May 14	May 30	Jun 15	Jul 1	Jul 16	Aug 2	Aug 18	Sep 3	Sep 19	Oct 5	average
1	1.68	2.00	3.20	3.15	3.38	3.68	4.94	6.00	4.25	3.00	
PM 10	1.68	2.00	3.00	3.07	3.38	3.68	4.73	5.91	4.25	3.00	3.47
PM 11	1.05	1.85	3.20	3.15	2.99	3.25	4.94	6.00	3.92	2.59	3.29
2	6.00	5.67	5.69	5.19	5.29	4.89	5.89	6.85	7.79	5.22	
PM 1	4.85	4.59	4.68	4.08	4.18	4.26	4.60	5.99	4.37	3.73	4.53
PM 4	5.36	5.32	5.49	5.19	5.29	4.69	5.89	6.65	4.84	5.22	5.39
PM 7	6.00	5.67	5.69	4.84	4.53	4.89	5.63	6.85	7.79	3.83	5.57
3	5.49	5.07	4.81	4.08	4.31	3.83	4.88	5.45	4.96	4.99	
PM 2	5.49	5.07	4.81	3.00	2.69	3.04	4.61	4.80	4.09	4.26	4.19
PM 3	4.16	4.08	4.49	3.81	3.30	3.31	4.28	4.96	4.16	3.67	4.05
PM 5	4.18	4.20	4.30	4.08	4.31	3.83	4.88	5.45	4.96	4.99	4.52
4	5.88	5.66	5.62	5.27	4.97	3.46	3.92	4.92	5.23	5.49	
PM 6	5.88	5.66	5.62	5.27	4.87	3.46	3.22	3.89	4.86	5.49	4.82
PM 8	5.22	5.27	5.22	4.90	4.97	3.28	3.92	4.92	5.23	2.84	4.58
PM 9	5.41	5.14	5.03	4.63	2.70	2.12	3.26	4.72	4.87	3.28	4.11

Model reliability

The statistics analyzed in Table 5 yielded an RMSE of 0.30, suggesting an error margin nearing zero (Cabrera, 2017). Additionally, the R^2 value was 0.95, indicating a strong correlation to a perfect linear fit (Martinez, 2005), and a NASH score of 0.92, signifying an excellent model performance (Terrazas, 2016).

The information in this article can be found in the following supplementary material link.

Figure 7 - Evaluation of the monitoring points, through cluster analysis with the k-means method (a), hierarchical dendrogram based on the ward.D2 method (b), cross-correlation (c), through which 4 groups with similar ET behaviors are identified in the phenological period of the starchy corn crop

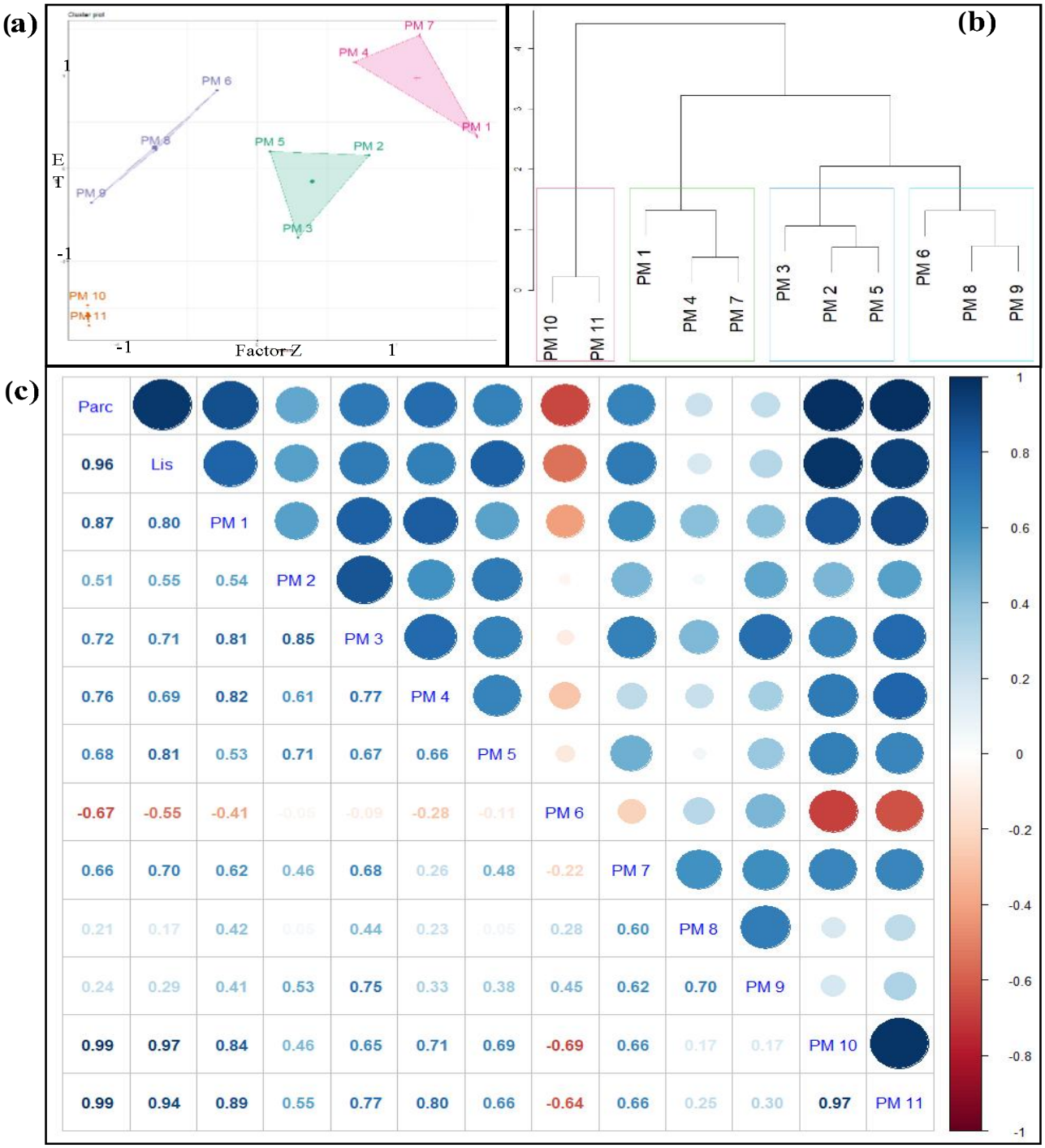

Figure 8 - Temporal variation of evapotranspiration (ET) from May to October in the lysimeter (Lis), experimental plot (Parc), and the 11 monitoring points (PM) from south to north of the province of Carhuaz PM1, PM2, PM3 to the province of Yungay PM4 to PM11. (a) ET between Parc and Lis during the beginning, development, middle, and end phenological period of starchy corn. (b) ET in Group 1 consisting of PM10 and PM11 installed with starchy corn. (c) ET in Group 2 consisting of PM1, PM4, and PM7 installed with green-grain starchy corn at elevations greater than 2550 m. (d) ET in Group 3 consisting of PM2, PM3, and PM5 installed with green starchy corn at elevations between 2450 to 2600 m, at latitudes greater than 9°10' S. (e) ET in Group 4 consisting of PM6, PM8, and PM9 installed with green-grain starchy corn, at latitudes lower than 9°10' S

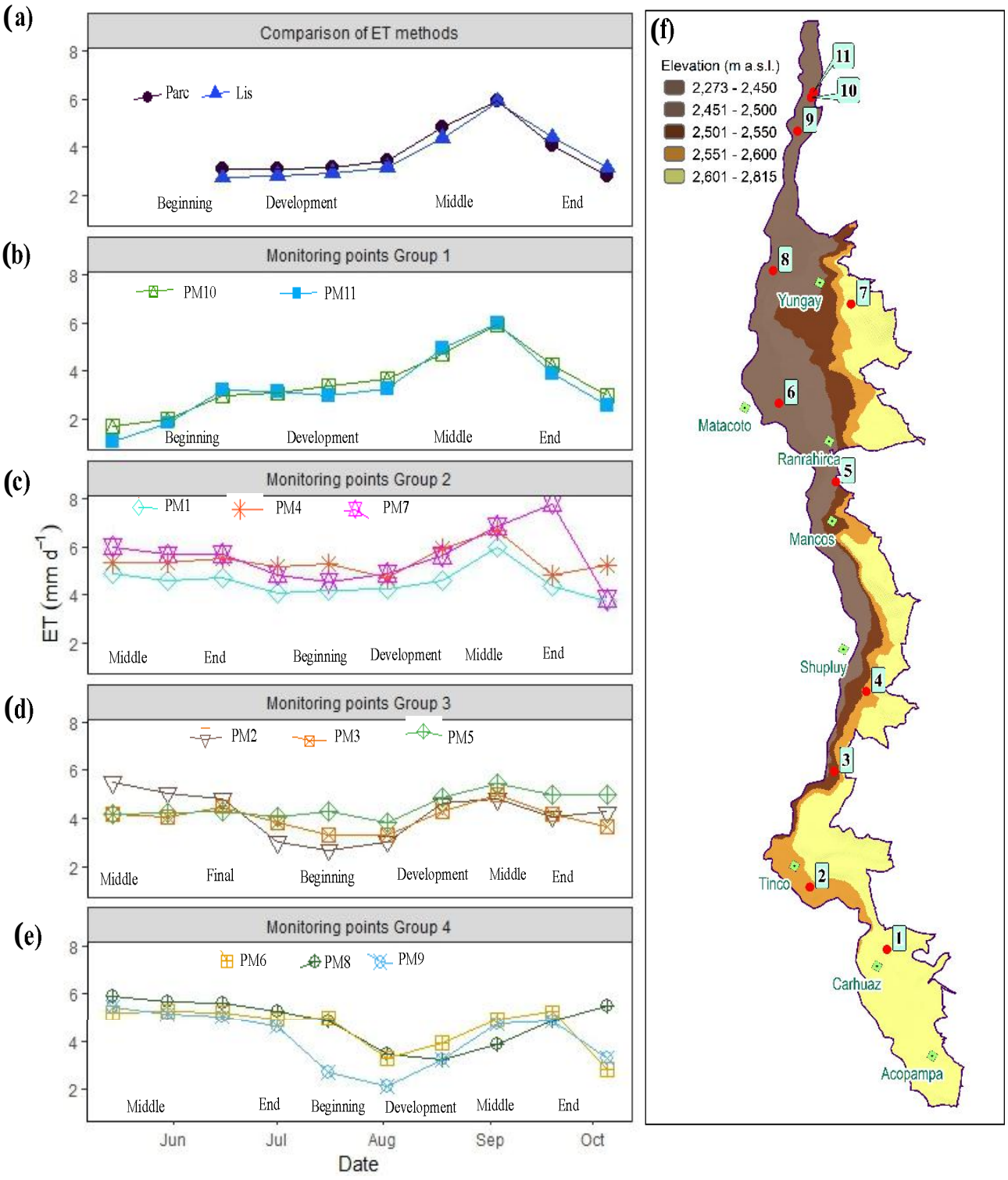

Figure 9 - Variation in average evapotranspiration (ET) of the four identified groups and according to the phenological development that includes the beginning (blue bars), development (orange bars), middle (grey bars), and end (yellow bars)

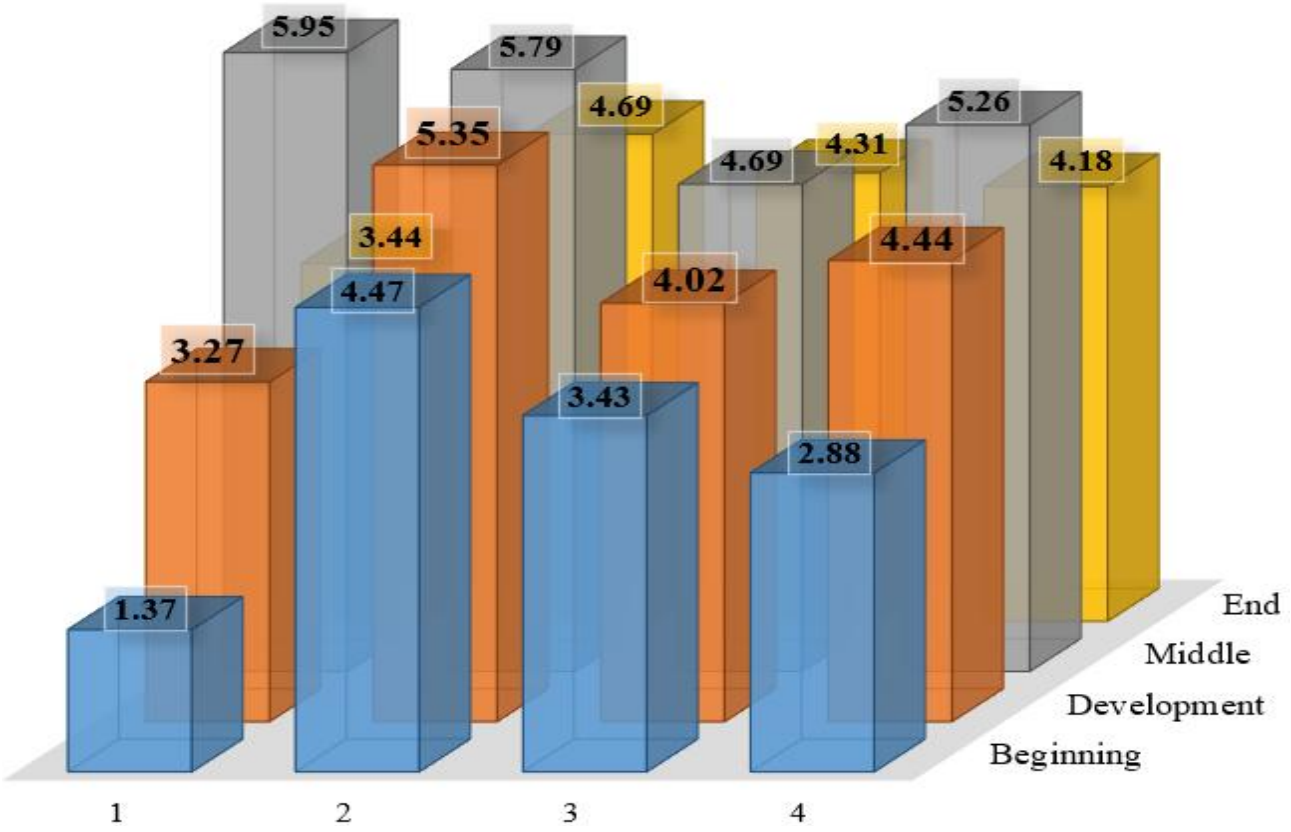

Table 5 - Statistical values of ET estimation with the SEBAL algorithm and measured with the drainage lysimeter

Statistics	Result
Percentage relative error (PRE)	0.09
Root mean square error (RMSE)	0.30
Coefficient of determination (R2)	0.92
Nash- Sutcliffe (NASH) efficiency	0.91

CONCLUSIONS

1. The spatio-temporal variability of the actual ET of starchy corn in a representative location in the Peruvian highlands was identified using the SEBAL algorithm and LANDSAT 8 satellite images. This variability depends on several factors such as elevation, latitude, radiation, phenology, and sowing date. In the Callejón de Huaylas;
2. The ET ranged from 1.05 mm d^{-1} to 7.79 mm d^{-1}. This analysis is essential for determining the water requirements of crops and provides vital information for individuals responsible for water resource management.

ACKNOWLEDGEMENTS

Special thanks to the Cañasbamba Research and Experimentation Center and the Environmental Research Center for Development (CIAD-FCAM) at the Santiago Antúnez de Mayolo National University. We are grateful to the engineers Esteban Reyes Roque and Rafael Tauquino Figueroa, Mr. Nuñubero, Dr. David Ramírez Collantes, PhD student Rebeca Salvador Reyes and the Research Unit of the National Agrarian University La Molina for their contributions to this research.

REFERENCES

ALI, A. *et al*. Satellite-based water and energy balance model for the arid region to determine evapotranspiration: development and application. **Sustainability**, v. 13, n. 23, p. 13111, 2021. DOI: https://doi.org/10.3390/su132313111.

ALLEN, R. G. *et al.* A Landsat-based energy balance and evapotranspiration model in Western US water rights regulation and planning. **Irrigation and Drainage Systems**, v. 19, n. 3/4, p. 251-268, 2005. DOI: https://doi.org/10.1007/s10795-005-5187-z.

ARYALEKSHMI, B. N. *et al*. Analysis of various surface energy balance models for evapotranspiration estimation using satellite data. **The Egyptian Journal of Remote Sensing and Space Science**, v. 24, n. 3, p. 1119-1126, 2021. DOI: https://doi.org/10.1016/j.ejrs.2021.11.007.

ASADI, M.; KAMRAN, K. V. Comparison of sebal, metric, and alarm algorithms for estimating actual evapotranspiration of wheat crop. **Theoretical and Applied Climatology**, 2022. Disponible en: https://link.springer.com/10.1007/s00704-022-04026-3. Accedido en: 30 abr. 2022.

BASTIAANSSEN, W. G. M. *et al*. A remote sensing surface energy balance algorithm for land (Sebal). 1. Formulation. **Journal of Hydrology**, v. 212/213, p. 198-212, 1998. DOI: https://doi.org/10.1016/S0022-1694(98)00253-4.

BENNIE, J. *et al.* Slope, aspect and climate: spatially explicit and implicit models of topographic microclimate in chalk grassland. **Ecological Modelling**, v. 216, n. 1, p. 47-59, 2008. DOI: https://doi.org/10.1016/j.ecolmodel.2008.04.010.

BURN, D. H.; HESCH, N. M. Trends in evaporation for the Canadian prairies. **Journal of Hydrology**, v. 336, n. 1/2, p. 61-73, 2007. DOI: https://doi.org/10.1016/j.jhydrol.2006.12.011.

CABRERA, J. **Calibración de modelos hidrológicos**. IMEFEN, 2017. Disponible en: http://www.imefen.uni.edu.pe/Temas_interes/modhidro_2.pdf. Accedido en: 30 jun. 2023.

CHA, M.; LI, M.; WANG, X. Estimation of seasonal evapotranspiration for crops in arid regions using multisource remote sensing images. **Remote Sensing**, v. 12, n. 15, p. 2398, 2020. DOI: https://doi.org/10.3390/rs12152398.

CUBAS, F. *et al*. **Evaluación de los modelos Cmip5 del Ipcc en el Perú**: proyecciones al año 2030 en la región Tacna, reporte ejecutivo del proyecto Pet 1194 fortalecimiento de capacidades regionales en la gestión del cambio climático, 2013. Disponible en: http://repositorio.senamhi.gob.pe/handle/20.500.12542/221#.XuusqN7L42g.mendeley. Accedido en: 30 jun. 2023.

DINPASHOH, Y. *et al.* Trends in reference crop evapotranspiration over Iran. **Journal of Hydrology**, v. 399, n. 3/4, p. 422-433, 2011. DOI: https://doi.org/10.1016/j.jhydrol.2011.01.021.

FERREIRA, P. M. D. L.; PAZ, A. R. D.; BRAVO, J. M. Objective functions used as performance metrics for hydrological models: state-of-the-art and critical analysis. **RBRH**, v. 25, p. 42, 2020. DOI: https://doi.org/10.1590/2318-0331.252020190155.

GARCIA, M. *et al*. Comparison of three operative models for estimating the surface water deficit using Aster reflective and thermal data. **Sensors**, v. 7, p. 860-883, 2007. DOI: https://doi.org/10.3390/s7060860.

GHADERI, A. *et al*. Estimation of actual evapotranspiration using the remote sensing method and Sebal algorithm: a case study in Ein Khosh plain, Iran. **Hydrology**, v. 7, n. 2, p. 36, 2020. DOI: https://doi.org/10.3390/hydrology7020036.

GOSHEHGIR, A. S.; GOLABI, M.; NASERI, A. A. Estimation and comparison actual evapotranspiration of sugarcane using separate and fusion satellite images and lysimeteric data with approach of determining water use efficiency. **Journal of the Indian Society of Remote Sensing**, v. 49, n. 6, p. 1461-1474, 2021. DOI: https://doi.org/10.1007/s12524-021-01326-5.

GUO, X. *et al*. Evaluating the potential of different evapotranspiration datasets for distributed hydrological model calibration. **Remote Sensing**, v. 14, n. 3, p. 629, 2022. DOI: https://doi.org/10.3390/rs14030629.

HU, X. *et al*. Comparison of physical-based, data-driven and hybrid modeling approaches for evapotranspiration estimation. **Journal of Hydrology**, v. 601, p. 126592, 2021. DOI: https://doi.org/10.1016/j.jhydrol.2021.126592.

KAMYAB, A. D.; MOKHTARI, S.; JAFARINIA, R. A comparative study in quantification of maize evapotranspiration for Iranian maize farm using Sebal and Metric-1 EEFLux algorithms. **Acta Geophysica**, v. 70, n. 1, p. 319-332, 2022. DOI: https://doi.org/10.1007/s11600-021-00704-4.

KIMBALL, B. A. Global change and water resources. *In*: LASCANO, R. J.; SOJKA, R. E. (ed.). **Irrigation of agricultural crops**. [*S. l.*]: John Wiley & Sons, 2015. p. 627-653. Disponible en: https://acsess.onlinelibrary.wiley.com/doi/abs/10.2134/agronmonogr30.2ed.c17. Accedido en: 20 sep. 2020.

KIPTALA, J. *et al.* Mapping ecological production and benefits from water consumed in agricultural and natural landscapes: a case study of the pangani basin. **Remote Sensing**, v. 10, n. 11, p. 1802, 2018. DOI: https://doi.org/10.3390/rs10111802.

LAIPELT, L. *et al*. Long-term monitoring of evapotranspiration using the Sebal algorithm and google earth engine cloud computing. **ISPRS Journal of Photogrammetry and Remote Sensing**, v. 178, p. 81-96, 2021. DOI: https://doi.org/10.1016/j.isprsjprs.2021.05.018.

LYLES, B. F. *et al.* Closing the water balance with a precision small-scale field lysimeter. **Sensors**, v. 24, n. 7, p. 2039, 2024. DOI: https://doi.org/10.3390/s24072039.

MARTINEZ, E. Errores frecuentes en la interpretación del coeficiente de determinación lineal. **Anuario Jurídico y Económico Escurialense**, v. 38, p. 16, 2005. Disponible en: https://dialnet.unirioja.es/servlet/articulo?codigo=1143023. Accedido en: 30 jun. 2023.

PAREDES, P. *et al*. Using the FAO dual crop coefficient approach to model water use and productivity of processing pea (*Pisum sativum* L.) as influenced by irrigation strategies. **Agricultural Water Management**, v. 189, p. 5-18, 2017. DOI: https://doi.org/10.1016/j.agwat.2017.04.010.

PERU. Ministerio de Desarrollo Agrario y Riego. **Perfil productivo y competitivo de los principales productos del sector en Perú**. 2022. Disponible en: https://siea.midagri.gob.pe/portal/siea_bi/index.html. Accedido en: 30 jun. 2023.

PRAKASH, M. M.; RAJITHA, K.; VARMA, M. R. R. Integration of soil moisture as an auxiliary parameter for the anchor pixel selection process in Sebal using Landsat 8 and Sentinel - 1A images. **International Journal of Remote Sensing**, v. 41, n. 3, p. 1214-1231, 2020. DOI: https://doi.org/10.1080/01431161.2019.1658239.

RAHIMZADEGAN, M.; JANANI, A. Estimating evapotranspiration of pistachio crop based on Sebal algorithm using Landsat 8 satellite imagery. **Agricultural Water Management**, v. 217, p. 383-390, 2019. DOI: https://doi.org/10.1016/j.agwat.2019.03.018.

RUIZ, J. A. *et al.* Cambio climático y sus implicaciones en cinco zonas productoras de maíz en México. **Revista Mexicana de Ciencias Agrícolas**, v. 2, n. 2, p. 309-323, 2011. Disponible en: http://www.scielo.org.mx/scielo.php?script=sci_abstract&pid=S2007-09342011000800011&lng=es&nrm=iso&tlng=es. Accedido en: 30 ene. 2023.

SHAMLOO, N. *et al.* Evapotranspiration estimation using Sebal algorithm integrated with remote sensing and experimental methods. **International Journal of Digital Earth**, v. 14, n. 11, p. 1638-1658, 2021. DOI: https://doi.org/10.1080/17538947.2021.1962996.

SOETEWEY, A. **Stats and R**. 2024. Disponible en: https://statsandr.com/blog/clustering-analysis-k-means-and-hierarchical-clustering-by-hand-and-in-r/. Accedido en: 21 may 2024.

TAN, L. *et al.* Evapotranspiration estimation using remote sensing technology based on a Sebal model in the upper reaches of the Huaihe river basin. **Atmosphere**, v. 12, n. 12, p. 1599, 2021. DOI: https://doi.org/10.3390/atmos12121599.

TERRAZAS, L. **Modelamiento hidrológico del río Zarumilla**. 2016. Disponible en: https://www.senamhi.gob.pe/load/file/01401SENA-35.pdf. Accedido en: 30 jun. 2023.

WATERS, R. *et al.* **Advanced training and user's manual of surface energy balance algorithms for land**. **Idaho Department of Water Resources**. 2002. Disponible en: https://www.posmet.ufv.br/wp-content/uploads/2016/09/MET-479-Waters-et-al-SEBAL.pdf. Accedido en: 10 jun. 2023.

WEI, G. *et al.* Spatial-temporal variation in paddy evapotranspiration in subtropical climate regions based on the Sebal model: a case study of the Ganfu plain irrigation system, southern China. **Remote Sensing**, v. 14, n. 5, p. 1201, 2022. DOI: https://doi.org/10.3390/rs14051201.

YANG, L. *et al*. Daily actual evapotranspiration estimation of different land use types based on Sebal model in the agro-pastoral ecotone of northwest China. **Plos One**, v. 17, n. 3, p. 265138, 2022. DOI: https://doi.org/10.1371/journal.pone.0265138.

ZHANG, X. *et al.* Evaluation of Most functions and roughness length parameterization on sensible heat flux measured by large aperture scintillometer over a corn field. **Agricultural and Forest Meteorology**, v. 150, n. 9, p. 1182-1191, 2010. DOI: https://doi.org/10.1016/j.agrformet.2010.05.003.